



Numerical solution of wetting fluid spread into porous media

Numerical solution of wetting fluid

B. Markicevic and H.K. Navaz

Department of Mechanical Engineering, Kettering University, Flint, Michigan, USA

521

Abstract

Purpose – The purpose of this paper is to develop a general numerical solution for the wetting fluid spread into porous media that can be used in solving of droplet spread into soils, printing applications, fuel cells, composite processing.

Design/methodology/approach – A discrete capillary network model based on micro-force balance is numerically implemented and the flow for an arbitrary capillary number can be solved. At the fluid interface, the boundary condition that accounts for the capillary pressure jump is used.

Findings – The wetting fluid spread into porous medium starts as a single-phase flow, and after some particular number of the porous medium characteristic length scales, the multi-phase flow pattern occurs. Hence, in the principal flow direction, the phase content (saturation) decreases, and in the lower limit for the capillary number sufficiently small, the saturation should become constant. This qualitative saturation behavior is observed irrespective of the flow dimensionality, whereas the quantitative results vary for different flow systems.

Research limitations/implications – The numerical solution has to be expanded to solve the spread of the fluid in the porous medium after there is no free fluid left at the porous medium surface.

Practical implications – It is shown that the multi-phase flow can develop even on a small domain due to the porous medium heterogeneity. Neglecting the medium heterogeneity and flow type can lead to a large error as shown for the droplet spread time in the porous medium.

Originality/value – This is believed to be the only paper relating to solving the droplet spread into porous medium as a multi-phase flow problem.

Keywords Porous materials, Fluid dynamics, Flow

Paper type Research paper

Received 10 September 2007
Revised 28 February 2008
Accepted 12 March 2008

Introduction

There is a variety of engineering applications ranging from oil recovery and soil flows to composites, printing, polymer filling, fuel cells in which the spread of the fluid phase into porous medium occurs (Holman *et al.*, 2002; Henz *et al.*, 2003; Neacsu *et al.*, 2007). These are multi-physics problems that involve momentum, heat and mass transport, where the structure of porous medium and the distribution of fluid phase that spreads into porous medium change, as well as the characteristic length scales (e.g. in oil recovery the length scale is in kilometers, whereas in printing it is less than a millimeter). In all these applications, a liquid phase spreads into porous medium (soil, concrete, paper), and the size of the liquid imprint is greatly influenced by whether the liquid spreads in the single- or multi-phase flow. Finally, the imprint size may be further altered by evaporation, adsorption, chemical reaction and/or external field (e.g. electromagnetic) that can take place in parallel with the momentum transport (Dinčov *et al.*, 2004; Zdražil *et al.*, 2006).

This project was collectively supported by The Air Force Research Laboratory, Human Effectiveness Directorate, Biosciences and Protection Division, Wright-Patterson AFB, The Defense Threat Reduction Agency (DTRA), and The US Army's Edgewood Chemical and Biological Center. The suggestions on the development of the technical framework from Dr J. Savage, Mr W. Kilpatrick and Dr T. D'Onofrio are greatly appreciated.



In order to predict the liquid spread accurately, the physical processes have to be defined and the flow type has to be determined. In respect to the momentum transport, there are three major physical processes that occur during the liquid spread: (i) change in shape of the contact area of the liquid that lays on the porous medium surface (inlet boundary), (ii) existence of the fully and partially saturated porous medium regions within the porous medium and the geometrical extent of these two regions, and (iii) secondary spread in which the liquid phase is transported from a fully to a partially saturated region, where the secondary spread takes place even when there is no liquid left on the porous medium surface. In some applications, the solution of all of these processes do not need to be included as for constant area inlet boundary; or for nearly homogeneous porous medium the spread can be solved as a single-phase flow problem. The secondary spread which is a very slow process can be neglected if the rate of the process that opposes the spread is sufficiently high (e.g. rate of evaporation).

The droplet spread into porous medium is one of the examples, where all three processes (i)-(iii) can exist. The shape of the sessile droplet that spreads into thin porous medium shows a large variation of the droplet base radius at the beginning and end of the spread, whereas in the middle of the spread, the base radius remains almost constant (Starov *et al.*, 2002; Starov, 2004). Using full numerical calculations for a three-dimensional porous medium, Alleborn *et al.* (2003) have come to a similar conclusion. The spread of the droplet is usually modeled setting the fully saturated and non-saturated region clearly separated (Reis *et al.*, 2004; Alleborn and Raszillier, 2004), without considering a partially saturated region of the porous medium. As droplet spread into porous medium is governed by viscous and capillary forces, and assuming the existence of the fully saturated region only, the droplet spread into a powder cannot be explained in full by influence of these two forces only (Popovich *et al.*, 1999). Using *MRI*, Mantle *et al.* (2003) have shown that the spread dynamics appears more complex with the fluid phase distributed between fully and partially saturated regions in porous medium, and so the droplet spread has to be modeled as a multi-phase flow problem.

Discrete pore network models provide a computational approach to elucidate transport of the liquid phase and can be used to evaluate transport parameters (Kohout *et al.*, 2006). In the network models, an actual porous medium is represented as a network of pores that are connected by throats (Fatt, 1956). For the liquid spread, the driving force is a resultant of the viscous, gravitational and capillary forces (Lenormand *et al.*, 1988). From these three forces, the potential threshold is defined (Prat, 1993) and the liquid distribution can follow single- or multi-phase flow pattern. From the known phase distribution, the multi-phase parameters can also be calculated (Constantinides and Payatakes, 1996), where the multi-phase parameters depend on phase content (saturation), emerging forces, solid/fluid contact angles, ratios of phase viscosities and flow rates, and the flow history as drainage or imbibition (Valavanides and Payatakes, 2001).

In this study, a general capillary network model is implemented and used to investigate the spread of the liquid phase into porous medium and the transition from single- to multi-phase flow during liquid spread. These changes are investigated using the liquid phase content (saturation). Using the saturation, the importance of flow dimensionality and the influence of local medium heterogeneity on the development of multi-phase flow has been elucidated. Finally, the model is used in the investigation of the droplet spread time into the porous medium for single- and multi-phase flow and the influence of inlet and capillary pressures on the flow type developed.

Model formulation

The liquid spread into porous media is modeled coupling the mass and momentum balance from the continuity equation and the Darcy law, where the fluid superficial velocity (\mathbf{u}) and pressure (p) are calculated:

$$\nabla \cdot \mathbf{u} = 0 \quad (1)$$

$$\mathbf{u} = -\frac{\mathbf{K}}{\mu} \nabla p \quad (2)$$

where (μ) is the fluid viscosity and (\mathbf{K}) is the porous medium permeability that for an isotropic medium becomes a scalar value (K). The problem is usually solved coupling the mass and momentum balance obtaining the potential equation for pressure. Since there is the pressure reduction at the liquid free boundary due to the capillary pressure (Chandio and Webster, 2002), the pressure jump at the free boundary is set equal to:

$$p_{free} = p_{out} \pm p_c \quad (3)$$

in which “+” is for non-wetting fluid, and “-” is for wetting fluid. From the pressure solution, the change of the fluid volume occupying porous medium in time is found by integrating the velocity at the free interface:

$$\frac{dV}{dt} = \int_{S_{free}} u_{free} dS \quad (4)$$

The set of Equations (1)-(4) allows for solution of the liquid spread providing that the permeability (K) and the capillary pressure (p_c) are known. For single-phase flow (K) and (p_c) are constant, and in the multi-phase flow the same set of equations is used with the only difference that (K) and (p_c) depend on the phase content (saturation).

In the capillary network model, the porous medium is represented as a capillary network of pores that are interconnected with throats and the liquid spread into porous medium can be solved regardless whether it occurs as single- or multi-phase flow. The pores are storage elements, whereas the throats show flow resistance. To account for local medium heterogeneity, the pore and/or throat size randomly varies in the network. The conservation of the momentum is defined over the throat, and for the cylindrical throat of radius (r_t) and length (l_t) that connects the pores (i) and (j), the flow rate from the Poiseuille flow can be written as:

$$q_{i,j} = \frac{\pi r_{t,ij}^4}{8\mu l_{t,ij}} (p_j - p) = g_{i,j} (p_j - p_i) \quad (5)$$

where ($g_{i,j}$) is the throat conductance, and the flow rate is defined into pore (i). Having the flow rate through one throat defined, the conservation of the mass at one pore (i) can be written, where the sum of all flow rates is equal to zero.

$$\sum_{1 \leq j \leq c} q_{i,j} = 0 \quad (6)$$

Each pore is connected to some number of neighboring pores that is defined as a pore coordination number (c). The coordination number of the flow pattern may differ from the network coordination number as clusters of originally present phase are formed during the liquid spread into the network. Furthermore, for the pore that is next to the pore at the interface, balance in Equation (5) is changed, where the pressure (p_j) is replaced by pertinent pressure value. For the inlet boundary, the pressure (p_j) becomes inlet pressure (p_{in}). The pressure of the originally present phase in the pore at the free interface is equal to the outlet pressure (p_{out}), whereas in the same pore the pressure in the liquid phase is reduced for the capillary pressure:

$$p_{free} = \frac{p_{out} - p_c = p_{out} - 2\sigma}{r_{t,free}} \quad (7)$$

with (σ) is the surface tension and the capillary pressure is calculated from Laplace–Young equation assuming the contact angle (θ) is equal to zero. Hence, for the pore next to the interface, (p_j) is replaced by (p_{free}). Finally, the balances for each pore are assembled obtaining a linear system of algebraic equation, $\mathbf{A} \times \mathbf{p} = \mathbf{b}$, from which the pressure in the liquid phase is calculated.

Having solved for the liquid phase pressure, the flow rates of pores at the interface can be calculated, and the flow rate for one pore at the free interface reads as:

$$q_{free} = - \sum_{1 \leq i \leq c_{free}} g_i (p_{out} - p_{c,i} - p_i) \quad (8)$$

where (c_{free}) is the number of throats occupied by liquid phase. Due to the capillary instability the interface pores can be both filled and emptied depending on the pressures of the surrounding pores that are filled by spreading liquid. From the pore volume (V_p), pore volume fraction that is filled by liquid that is referred to as pore saturation (s), and the flow rate into the pore (can be either positive or negative), the time needed to fill/empty any of the pores at the interface can be calculated:

$$t = \begin{cases} (1-s)V_p/q_{free}, & \text{fill} \\ -sV_p/q_{free}, & \text{empty} \end{cases} \quad (9)$$

From calculating the fill/empty times for all pores at the interface (t_i), ($1 \leq i \leq n_{free}$), the time of the discrete step for which one pore changes its “state” is found as a minimum time:

$$t_{step} = \min_{1 \leq i \leq n_{free}} \{t_i\} \quad (10)$$

and from time step (t_{step}), the changes of the pore saturation is determined. Finally, the volume of the fluid (V_{step}) that flows into the porous medium for particular step is found as:

$$V_{step} = t_{step} \sum_{1 \leq i \leq n_{free}} q_{free,i} \quad (11)$$

where ($q_{free,i}$) are flow rates into the pores at the free interface.

Numerical solution

Solving the liquid spread using the capillary network model consists of two parts, the first being the capillary network creation and the latter one is the flow solution on the network defined. A regular rectangular network consists of $(n_x \times n_y \times n_z)$ pores, with the coordination number (c) that is defined as a number of neighbors connected to one pore equal to four or six for two- and three-dimensional network, respectively. A numerical procedure for the network generation is developed and it is independent of the problem dimensionality, where for two-dimensional cases, the number of layers in (y) direction is set equal to one, $n_y = 1$. In the liquid spread, there are three parameters that need to be known, namely (ϕ, K, p_c) , that are related to the network parameters, (V_p, r_t, l_t) . If the volume of all the pores in the network (V_p) is equal, it can be calculated from the overall volume of porous medium (V_m), porosity (ϕ) and the network size $(n_x \times n_y \times n_z)$:

$$\frac{V_p = \phi V_m}{(n_x n_y n_z)} \quad (12)$$

If the pore volume is variable and prescribed with the distribution function, the sum of all the pore volumes has to be equal to the porous medium void volume (ϕV_m). The remaining two parameters (p_c) and (K) are set by adjusting throat parameters: radius (r_t) and length (l_t), where the throat radius is randomly distributed and it is found such to satisfy the capillary pressure, and (l_t) is found adjusting the network permeability. An additional network parameter that can be used to adjust (p_c) and (K) is the network coordination number that can be set to vary in the network (Hilpert *et al.*, 2003; Ioannidis and Chatzis, 1993).

A general capillary network solution of the liquid spread is implemented for arbitrary network dimensionality, coordination number and flow capillary number (defined as a ratio of viscous and capillary force). In the solution, the numerical procedure for the cluster identification is based on the cluster definition that it is a part of the network occupied with the originally present phase from which network inlet or outlet can not be reached without using the pores/throats occupied with the spreading liquid. The influence of the capillary number is given through the flow rate in the pore at the free interface given in Equation (8), where the contribution of both capillary and viscous force is included. As the liquid spreads into the network, the number of pores filled with liquid increases and the system matrix (\mathbf{A}) becomes larger. However, (\mathbf{A}) changes only in the part for the pore being filled or emptied, and therefore, (\mathbf{A}) is defined as a dynamic array that is updated only for the pores that are altered in the current step. Finally, in the code the mass conservation is checked in each step and from the integral mass balance one can write:

$$\int_{S_{inl}} u_{inl} dS = - \int_{S_{free}} u_{free} dS \quad (13)$$

where the flow rate across inlet boundary (S_{inl}) has to be equal to the flow across the free interface (S_{free}).

Results and discussion

Unidirectional spread into two- and three-dimensional networks, unidirectional radial spread into two-dimensional network and the sessile droplet spreads are solved, and

the changes in the saturation profile and spread time are investigated. All spreads are solved for the non-changing area of the inlet boundary. The droplet spread is also solved for a variable capillary number. Using Equation (13) the mass conservation is checked, where the relative error calculated from the flow rate across the inlet boundary (Q_{inl}) and free interface (Q_{free}) as $(1-Q_{free}/Q_{inl})$ is in the order of 10^{-10} . In all calculations, using a random number generator the throat radii were uniformly distributed in the range (r_{min}, r_{max}) , with the heterogeneity parameter, $\chi = r_{max}/r_{min} - 1$. Other throat radius distributions (e.g. normal, *log*-normal, binomial) can easily be prescribed in the numerical solver. In this study, the uniform distribution is used in order to introduce the medium local heterogeneity that is responsible for emerging of a multi-phase flow scenario. It should be noted that other forms of distributions will also produce a multi-phase flow pattern with a different saturation profile along principal flow direction and transport parameters (capillary pressure and phase permeability). These characteristics can be used in constructing the network that represents an actual porous medium. Without actual numerical simulations, it is hard to predict how the throat size distribution influences multi-phase flow development and transport parameters. By using a different distribution the fraction of small (or large) throats is changed therefore altering the process rate and fluid behavior at the free interface (e.g. using *log*-normal distribution instead of the uniform one the fraction of small throats increases). Finally, for the capillary driven flow, the pressures at the inlet and outlet boundaries are kept equal, $p_{inl} = p_{out}$ and the influence of viscous force on the droplet spread is investigated by gradually increasing (p_{inl}).

Unidirectional flows

Two-dimensional network of $n_x \times n_y \times n_z = 100 \times 1 \times 100$ is constructed, with the radius of inlet equal to $r_0 = n_x/10$ placed in the domain center, and the medium heterogeneity (χ) is varied from 0.1 to 14. In Figure 1(a)-(d), the flow patterns for four different (χ) of the spreading phase are shown (black color), and the part of the medium

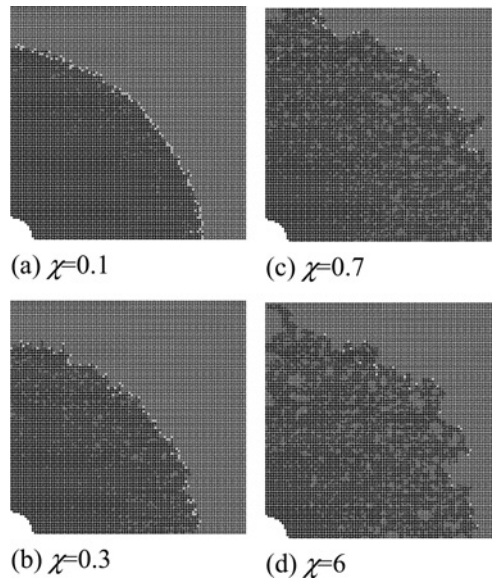


Figure 1. Radial spread for different heterogeneous media over the network of $n_x = n_z = 100$, where spreading phase is given in black color. The clusters of originally present phase become larger and the flow front becomes more irregular

that the spreading liquid does not reach and the entrapped originally present phase (clusters) are shown with dark grey color. It can be seen that the free interface becomes more irregular as heterogeneity increases, where for low (χ) the free interface is smooth. The local potential of the spreading phase causes this irregularity at the flow front, and only some pores at the free interface can be accessed by spreading liquid. In Figure 1(a)-(d), these pores are depicted in light grey color, and their number is reduced as (χ) increases. Hence, it is evident that the spreading liquid saturation profile will decrease faster as medium heterogeneity (χ) increases. This is shown in Figure 2, where the radial saturation profiles for five different (χ) are plotted. It can be seen that for low (χ), the saturation remains very close to one, whereas for higher (χ) saturation decreases to as low as 0.75. However, the saturation did not reach its constant value and after 60 pores along radial principal flow direction the saturation profile is still developing.

In order to find whether the saturation reaches the constant value, the radial spread is solved on the larger network of $n_x \times n_y \times n_z = 400 \times 1 \times 400$ and $r_0 = n_x/10$. Figure 3 shows the numerical results:

- phase distribution; and
- saturation profile.

The saturation profile in Figure 3(b) is averaged for two different radial increments (Δr): in total 30 (solid line) and 90 (dashed line) radial slices. The numerical solution shows that the saturations gradient decreases, but even after $r_f > 350$ pores the saturation does not become constant. Here, the smallest saturation, $s \approx 0.65$ is reached. To further increase the number of pores along which spread takes place, two-dimensional network $n_x \times n_y \times n_z = 60 \times 1 \times 600$ is constructed, where the phase spreads along (n_z) direction, and the fluid inlet is placed along (n_x) boundary. Taking $n_x = 60$, the network should be sufficiently large to reduce the edge effects caused by clusters. The distribution of phases: spreading and originally present one is shown in Figure 4 with black and dark grey colors, respectively. In Figure 4(a), the whole network is depicted, and Figure 4(b) shows a part of the domain only. The saturation profiles are shown in Figure 5, where the averaged saturation for ($z = \text{const.}$) and ($\Delta z = \text{const.}$) are depicted with dashed double dotted and solid lines, respectively. It can be observed that the saturation indeed decreases for the first 450 pores, and the numerical calculations with larger network should be undertaken in order to check the saturation profile for $z > 450$.

Using the two-dimensional network, the spread of the liquid is restricted, as clusters are two-dimensional objects. Therefore, the computation of the unidirectional fluid

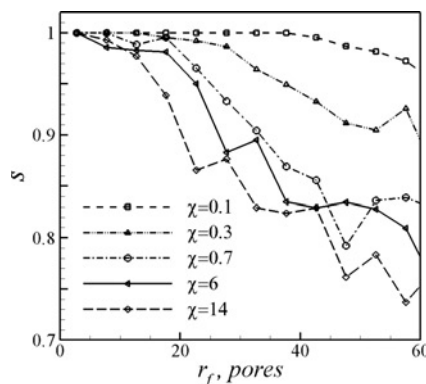


Figure 2.
Radial saturation profiles
for spreads in different
heterogeneous media

Figure 3. Radial spread into larger network of $n_x = n_z = 400$ and heterogeneity $\chi = 0.7$: (a) distribution of phases, where spreading phase is shown with black color, and (b) radial saturation profile. Two profiles are obtained for radius divided into 30 and 90 radial slices

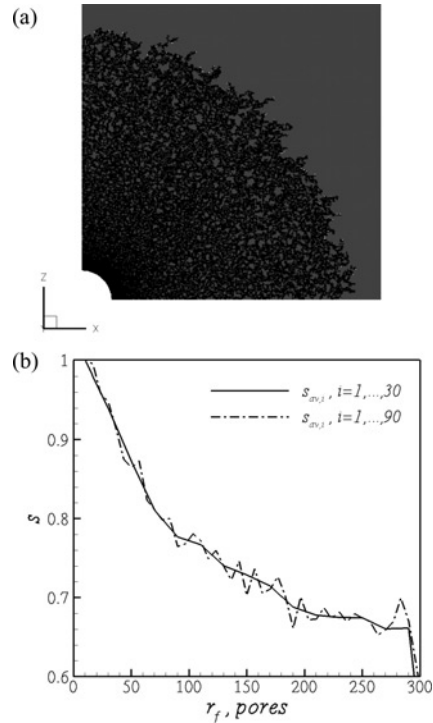
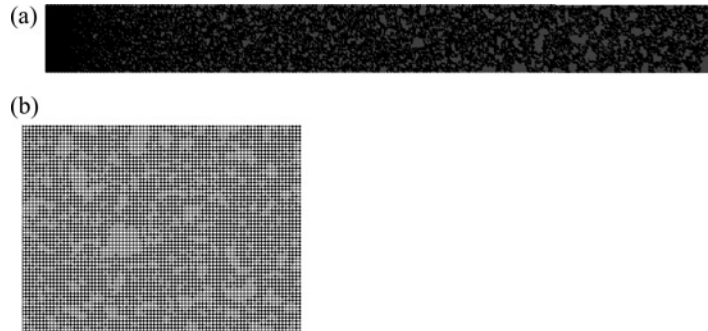


Figure 4. Unidirectional spread of the fluid into rectangular two-dimensional network, $n_x \times n_z = 60 \times 600$. The maximum clusters size increases up to ten pores. In figure (b), a small part of the network is depicted



spread is repeated, but using the three-dimensional network, $n_x \times n_y \times n_z = 60 \times 10 \times 250$, where the fluid inlet is placed at $n_x n_y$ plane, and again, the flow takes place in (z) direction. The originally present phase clusters are visualized and shown in Figure 6(a). There are no clusters of originally present phase close to the domain inlet, and they are formed and increase in size down the flow direction (depicted as light grey color inclusions). The saturation change as a function of (z) is shown in Figure 6(b). As in two-dimensional networks, the saturation of the spreading phase close to the inlet is equal to one, and it decreases downstream. In Figure 7, the saturation profiles for different unidirectional flows are compared for constant network heterogeneity, $\chi = 0.7$. The decrease of saturation is smallest for the three-dimensional

flow (dashed line) as network coordination number is larger (six compared to four) and the cluster size is smallest. Finally, the fastest decrease of the saturation is observed for radial flow that might be attributed to its diverging nature.

Droplet spread

Initially, the sessile droplet spread into homogeneous network (here, $r_{\min} = r_{\max}$ and $\chi = r_{\max}/r_{\min} - 1 = 0$) is solved, where the influence of the droplet base radius (r_0) is investigated. In the numerical calculations, a droplet of volume, $V_{d,0} = 30 \text{ mm}^3$ spreads into a network of $n_x \times n_y \times n_z = 60 \times 60 \times 60$ pores. In Figure 8, the shapes of the droplet at the central plane for two droplet base radii $r_0 = n_x/6$ and

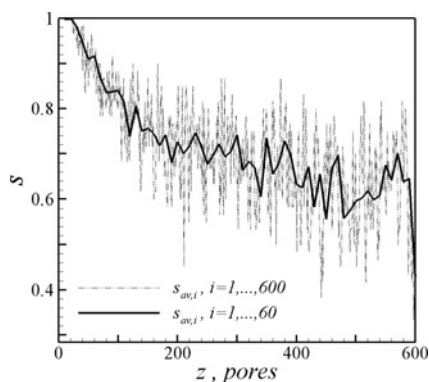


Figure 5.
Saturation profile in rectangular network averaged over two different network segments: $z = \text{const}$ double dotted dashed line and $\Delta z = \text{const}$. (solid line)

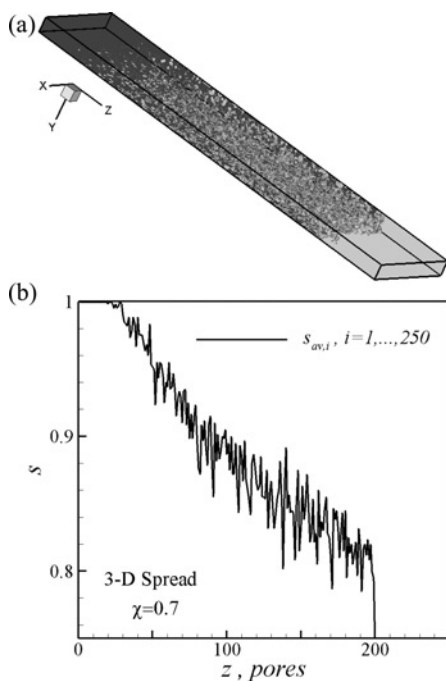


Figure 6.
Unidirectional spread of the fluid into rectangular three-dimensional network, $n_x \times n_y \times n_z = 60 \times 10 \times 250$: (a) phase distribution with the clusters of originally present phase shown in light gray color, and (b) saturation profile

$r_0 = n_x/2$ are depicted with dashed dotted and solid lines, respectively. The penetration depth is larger for $r_0 = n_x/6$, and the spread time for $r_0 = n_x/6$ droplet is an order of magnitude longer compared to $r_0 = n_x/2$ droplet. The numerical simulations of the same two drops are repeated, but representing the porous medium as a heterogeneous one, with $\chi = 0.7$. The results of the droplet spreads are shown in Figures 9(a) and (b) for $r_0 = n_x/2$ and $r_0 = n_x/6$, respectively. In Figure 9(a), only 40 pores in (z) direction are depicted. There are large differences in flow patterns for two different droplet base radii, $r_0 = n_x/6$ and $r_0 = n_x/2$. The droplet spread for $r_0 = n_x/2$ remains close to the single-phase flow, whereas multi-phase flow for $r_0 = n_x/6$ droplet spread is observed. In order to better visualize the flow type, an arbitrary yOz plane is depicted in Figure 9 also. For $r_0 = n_x/2$, a few clusters of originally present phase can be observed. On the other hand, there is a large number of clusters for $r_0 = n_x/6$ that appear at the some distance from the inlet and as similar to unidirectional flows, the clusters increase in number and size as droplet spreads further into the network. The multi-phase flow development is caused by the spread rate and for slower spread ($r_0 = n_x/6$), even a droplet of volume less than $V_d = 30 \text{ mm}^3$ will spread in the multi-phase flow.

The times it takes for the droplet to spread for both homogeneous ($\chi = 0$) and heterogeneous ($\chi > 0$) networks are calculated. Additionally, the time changes of:

- flow rates across droplet base (inlet) (Q); and
- droplet remaining volume on the porous medium surface ($V_{d,free}$) are calculated.

Figure 7.
Influence of dimensionality and flow type on saturation profile. The size of three-dimensional clusters is reduced, whereas radial flow promotes large clusters formation

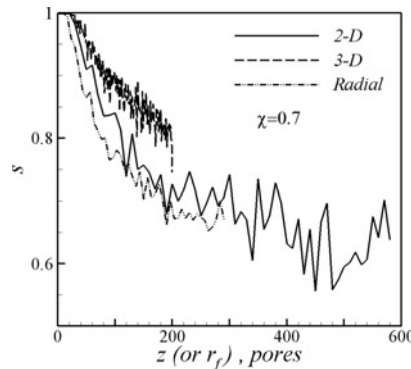
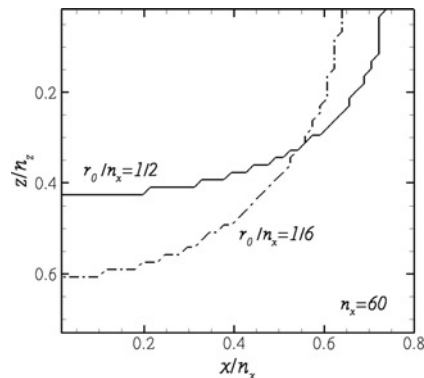


Figure 8.
The spread of droplet of constant volume into homogeneous porous medium $n_x \times n_y \times n_z = 60 \times 60 \times 60$ for two different droplet base radii (r_0), $r_0 = n_x/2$ (solid line), and $r_0 = n_x/6$ (dashed dotted line)



It is well known (De Wit, 1995) that the permeability (K) of *log*-normally distributed heterogeneous medium that is referred to as effective permeability is smaller compared to the permeability of a homogeneous sample. For one- and two-dimensional flows the effective permeability is equal to the harmonic (K_H) and geometric (K_G) mean of local permeabilities, respectively. Replacing the actual medium with a homogeneous one and setting its effective permeability to be equal to the arithmetic mean (K_A) produces an error according to ($K_A \geq K_G \geq K_H$), where the equal sign is only true for a homogeneous sample. Using numerical calculations, it has also been shown that for uniformly distributed heterogeneous medium the effective permeability decreases as the medium heterogeneity increases (Markicevic *et al.*, 2007). Therefore, the spread time increases for heterogeneous network. Figure 10 shows the changes of (Q) and ($V_{d,free}$) in time for $r_0 = n_x/2$ and both homogeneous (solid lines) and heterogeneous (dashed double dotted lines). The spread time is calculated from $V_{d,free} = 0$, where it can be seen from Figure 10 that the spread time is longer for heterogeneous ($\chi > 0$) sample of around 20 per cent. The spread of droplet $V_d = 30 \text{ mm}^3$ and $r_0 = n_x/6$ occurs as a multi-phase flow (see Figure 9(b)), and modeling the actual ($\chi > 0$) network by homogeneous one ($\chi = 0$) will produce a larger error than in the previous case (Figure 9(a)). The changes of (Q) and ($V_{d,free}$) in time are shown in Figure 11. At first glance, a stark difference in spread times can be observed, where $t_{s,heter} \approx 2 \times t_{s,hom}$. This finding ($t_{s,heter} \approx 2 \times t_{s,hom}$) implies that the influence of the multi-phase transport is much higher compared to the heterogeneity influence in single-phase flow (refer to Figure 10, where $t_{s,heter} \approx 1.2 \times t_{s,hom}$).

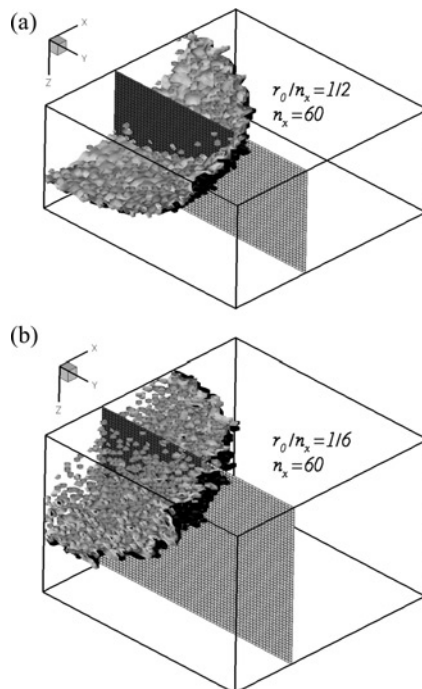


Figure 9.
The spreading phase distribution and originally present phase clusters (light gray color) for droplet spread into heterogeneous medium, $\chi = 0.7$ and two droplet base radii (r_0): (a) $r_0 = n_x/2$, where single-phase flow is observed, and (b) $r_0 = n_x/6$, with multi-phase flow developed

Finally, the influence of the viscous and capillary forces on the rate of droplet spread is investigated for a sessile droplet that spreads in the multi-phase flow (as one in Figure 9(b)). Setting the liquid surface tension equal to zero ($\sigma = 0$), the capillary force is excluded and the spread time is influenced by viscous force only. The ratio between viscous and capillary force is altered by keeping ($\sigma \neq 0$) and changing the inlet pressure (p_{in}). It is obvious that for ($p_{in} = p_{out}$), the spread of the sessile droplet is under the capillary force only. The changes of flow rate at the inlet boundary (Q) in time are shown in Figure 12, where pairs ($\sigma = 0$ and $\sigma \neq 0$) of curves are given except

Figure 10. Changes of the remaining droplet volume on porous medium surface ($V_{d,free}$), and the flow rate into porous medium (Q) for $r_0 = n_x/2$ for homogeneous (solid lines), and heterogeneous (dashed dotted lines) porous medium

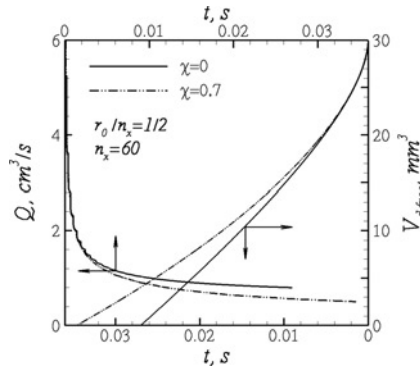


Figure 11. Changes of the remaining droplet volume on porous medium surface ($V_{d,free}$), and the flow rate into porous medium (Q) for $r_0 = n_x/6$ for homogeneous (solid lines), and heterogeneous (dashed dotted lines) porous medium

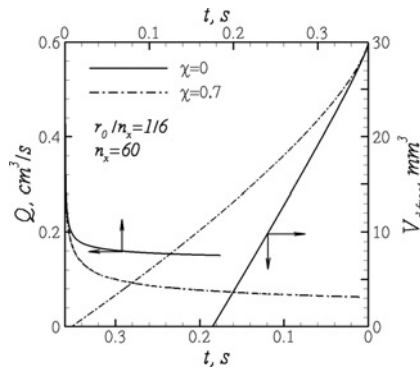
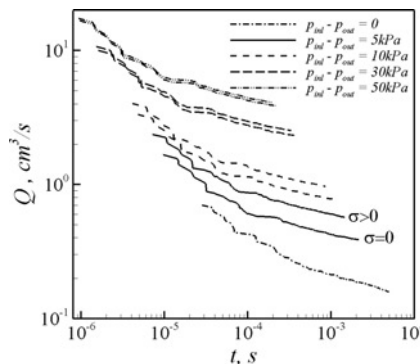


Figure 12. Influence of capillary and viscous force on the droplet spread rate and spread time



for ($p_{\text{inl}} = p_{\text{out}}$) condition. It can be seen that for a sufficiently high viscous force (high flow rate), the capillary force can be neglected and curves ($\sigma = 0$) and ($\sigma \neq 0$) almost coincide. The curves ($Q \sim t$) cannot be collapsed on the same dependence as with the increase of spread rate, the spread changes from multi-phase to the single-phase flow due to the flow stabilization.

Conclusions

The capillary network model that accounts for the capillary pressure jump at the free interface is developed and used to study the spread of the wetting fluid into porous medium. Both homogeneous and heterogeneous media flow can be solved. For the spread into heterogeneous medium it is found that the flow dimensionality, local heterogeneity and distance from the inlet influence the saturation. Irrespective from the medium heterogeneity, the fluid saturation remains almost equal to one in the part of the medium close to the inlet and it decreases in the principal flow direction as spread becomes slower. Even for single-phase flow, the fluid spread in a heterogeneous medium differs from its counterpart in a homogeneous sample, where it is found that the spread time is longer for a heterogeneous sample. In the heterogeneous medium, the free interface is not smooth as a result of the local changes in the porous medium structure and the flow front of a particular width is formed. Once the flow front at the free interface becomes sufficiently broad, the separate flow paths within the flow front can merge and the clusters of originally present phase are formed and multi-phase flow occurs. The transition from single- to multi-phase flow is investigated, where it is found that the droplet of the same volume can spread in the single- or multi-phase flow depending on the process rate. This finding is corroborated by investigating the droplet spread for different inlet pressures (capillary number), where for the faster spread (higher inlet pressure), the transition from single- to multi-phase flow occurs later as a result of the flow stabilization.

References

- Alleborn, N. and Rasziller, H. (2004), "Spreading and sorption of a droplet on a porous substrate", *Chemical Engineering Science*, Vol. 59, pp. 2071-88.
- Alleborn, N., Rasziller, H., Anthonissen, K. and Lievens, O. (2003), "Spreading and sorption of a droplet on a porous substrate", Fifth European Coating Symposium, Fribourg, pp. 246-51.
- Chandio, M.S. and Webster, M.F. (2002), "Numerical simulation for viscous free-surface flows for reverse-roller coating", *International Journal of Numerical Methods for Heat and Fluid Flow*, Vol. 12, pp. 434-57.
- Constantinides, G.N. and Payatakes, A.C. (1996), "Network simulation of steady-state two-phase flow in consolidated porous media", *AIChE Journal*, Vol. 42, pp. 369-82.
- De Wit, A. (1995), "Correlation structure dependence of the effective permeability of heterogeneous porous media", *Physics of Fluids*, Vol. 7, pp. 2553-62.
- Dinčov, D.D., Parrott, K.A. and Pericleous, K.A. (2004), "A new computational approach to microwave heating of two-phase porous materials", *International Journal of Numerical Methods for Heat and Fluid Flow*, Vol. 14, pp. 783-802.
- Fatt, I. (1956), "The network model of porous media III. Dynamic properties of networks with tube radius distribution", *Trans AIME*, Vol. 207, pp. 164-81.
- Henz, B.J., Tamma, K.K., Kanapady, R., Ngo, N.D. and Chung, P.W. (2003), "Process modeling of composites by resin transfer molding: practical applications of sensitivity analysis for isothermal considerations", *International Journal of Numerical Methods for Heat and Fluid Flow*, Vol. 13, pp. 415-47.

- Hilpert, M., Glantz, R. and Miller, C.T. (2003), "Calibration of a pore-network model by a pore-morphological analysis", *Transport in Porous Media*, Vol. 51, pp. 267-85.
- Holman, R.K., Cima, M.J., Uhland, S.A. and Sachs, E. (2002), "Spreading and infiltration of inkjet-printed polymer solution droplets on a porous substrate", *Journal of Colloid and Interface Science*, Vol. 249, pp. 432-40.
- Ioannidis, M.A. and Chatzis, I. (1993), "A mixed-percolation model of capillary hysteresis and entrapment in mercury porosimetry", *Journal of Colloid and Interface Science*, Vol. 161, pp. 278-91.
- Kohout, M., Grof, Z. and Stepanek, F. (2006), "Pore-scale modeling and tomographic visualisation of drying in granular media", *Journal of Colloid and Interface Science*, Vol. 299, pp. 342-51.
- Lenormand, R., Touboul, E. and Zarcone, C. (1988), "Numerical models and experiments on immiscible displacement in porous media", *Journal of Fluid Mechanics*, Vol. 189, pp. 165-87.
- Mantle, M.D., Reis, N.C., Griffiths, R.F. and Gladden, L.F. (2003), "MRI studies of the evaporation of a single liquid droplet from porous surfaces", *Magnetic Resonance Imaging*, Vol. 21, pp. 293-97.
- Markicevic, B., Bazylak, A. and Djilali, N. (2007), "Determination of transport parameters for multiphase flow in porous gas diffusion electrodes using a capillary network model", *Journal of Power Sources*, Vol. 171, pp. 706-17.
- Neacsu, V., Leisen, J., Beckham, H.W. and Advani, S.G. (2007), "Use of magnetic resonance imaging to visualize impregnation across aligned cylinders due to capillary forces", *Experiments in Fluids*, Vol. 42, pp. 425-40.
- Popovich, L.L., Feke, D.L. and Manas-Zloczower, I. (1999), "Influence of physical and interfacial characteristics on the wetting and spreading of fluids on powders", *Powder Technology*, Vol. 104, pp. 68-74.
- Prat, M. (1993), "Percolation model of drying under isothermal conditions in porous media", *International Journal of Multiphase Flow*, Vol. 19, pp. 691-704.
- Reis, N.C., Griffiths, R.F. and Santos, J.M. (2004), "Numerical simulation of the impact of liquid droplets on porous surfaces", *Journal of Computational Physics*, Vol. 198, pp. 747-70.
- Starov, V.M. (2004), "Surfactant solutions and porous substrates: spreading and imbibition", *Advances in Colloid and Interface Science*, Vol. 111, pp. 3-27.
- Starov, V.M., Kostvintsev, S.R., Sobolev, V.D., Velarde, M.G. and Zhdanov, S.A. (2002), "Spreading of liquid drops over dry porous layers: complete wetting case", *Journal of Colloid and Interface Science*, Vol. 252, pp. 397-408.
- Valavanides, M.S. and Payatakes, A.C. (2001), "True-to-mechanism model of steady-state two-phase flow in porous media, using decomposition into prototype flows", *Advances in Water Resources*, Vol. 24, pp. 385-407.
- Zadrazil, A., Stepanek, F. and Matar, O.K. (2006), "Droplet spreading, imbibition and solidification on porous media", *Journal of Fluid Mechanics*, Vol. 562, pp. 1-33.

Corresponding author

B. Markicevic can be contacted at: bmarkice@kettering.edu